35th Annual International Conference of the IEEE EMBS
Osaka, Japan, 3 - 7 July, 2013

An Automatic Brain Tumor Segmentation Tool

Idanis Diaz[1,4], Pierre Boulanger[1], Russell Greiner[1,2], Bret Hoehn[1,2], Lindsay Rowe[3], and Albert Murtha[3]

Abstract— **This paper introduces an automatic brain tumor segmentation method (ABTS) for segmenting multiple components of brain tumor using four magnetic resonance image modalities. ABTS's four stages involve automatic histogram multi-thresholding and morphological operations including geodesic dilation. Our empirical results, on 16 real tumors, show that ABTS works very effectively, achieving a Dice accuracy compared to expert segmentation of 81% in segmenting edema and 85% in segmenting gross tumor volume (GTV).**

I. INTRODUCTION

Medical image segmentation provides information necessary for diagnosis, radiotherapy, treatment planning and assessment, disease monitoring and surgery planning. This paper focuses on segmenting brain tumors in magnetic resonance (MR) images, to distinguishe different components within the tumor volume.

In typical clinical practice, experts *manually* segment a volume, or use semi-automated tools. Unfortunately, such manual segmentation of tumors is time consuming and yields non-repeatable results [1]. Many semi-automatic tumor segmentation approaches have been reported in the literature [2], [3], [4]; however, few of these methods achieve the objectives most desired in clinical practices: simplicity, accuracy, speed, and minimal user interaction. Some semi-automatic segmentation methods are based on elementary image processing techniques, for example, thresholding, region growing, and edge detection. Some of these methods require extensive user interactions and their accuracy is reduced by the lack of contrast at the boundaries between different tissues. Methods that involve robust statistical models or machine learning techniques, for instance, fuzzy clustering and k-nearest-neighbor, require precise input parameters and user result interpretations [2], [3], [4]. Other methods, based on deformable models, are very sensitive to the inhomogeneities present in the images and also require user guidance.

This paper presents the Automatic Brain Tumor Segmentation (ABTS) algorithm, which is efficient, does not require a user to provide input parameters nor initial estimates, nor require any other user interaction, and also is very simple to use. Our approach finds edema and gross tumor volume (GTV) using four standard 2D magnetic resonance sequences: T1-weighted spin-echo (T1), T1-weighted spin echo with gadolinium contrast agent (T1C), T2-weighted spin echo (T2) and Fluid Attenuated Inversion Recovery (FLAIR) [5]. Our approach uses an automatic histogram multi-thresholding procedure and morphological operations, including geodesic transformations [6]. Although segmentation methods based on histograms are very sensitive to the poor contrast at the tissue boundaries, ABTS overcomes this challenge by using the information provided by the different scans and with the use of double-thresholding at different grey levels and geodesic dilation.

Section II describes our ABTS segmentation method; each of its subsections explaining one component of its components. Section III shows that ABTS works effectively on real MR images, producing results comparable to expert manual segmentations.

II. THE ABTS SEGMENTATION ALGORITHM

Our ABTS segmentation algorithm takes as input four registered images of the same patient containing the four standard MR sequences: T1, T1C, T2 and FLAIR. Then, ABTS applies the following steps:

A. Thresholding

In this first stage, ABTS takes advantage of the known histogram shapes common to the vast majority of brain MRI scans. Generally, brain MRI histograms are bimodal: the first mode represents the most common intensity values found in the image background, which are close to zero; and the second mode is mostly composed of grey values found in brain tissues corresponding to gray and white matter (see Figure 1). We followed Brummer *et al.* [7] by localizing different thresholds in the four image histograms to obtain binary 3D masks designed to separate different regions of interest within the image – *e.g.*, background from foreground, or the skull from brain tissue or affected areas with high/low intensities from healthy tissues. In order to simplify the threshold localization, our approach uses a Savitzky-Golay FIR filter to obtain smooth histogram envelopes for each volume [8]. This filter preserves higher-order moments by approximating the data within a window with a high-order polynomial using a least-squares procedure [9].

* This work was developed in the mark of the Brain Tumor Analysis Project, a collaboration between the University of Alberta's Computing Science Department and Cross Cancer Institute. The project is sponsored by the Terry Fox Research Institute, the Alberta Cancer Foundation, Alberta Innovates Centre for Machine Learning, and NSERC.

[1]I. Diaz, P. Boulanger, R. Greiner and B. Hoehn are with the Department of Computing Science, University of Alberta.

[2] R. Greiner and B. Hoehn are also with the Alberta Innovates Centre for Machine Learning.

[3]L. Rowe and A. Murtha are at Radiation Oncology Department at the Cross Cancer Institute, Alberta.

[4]I. Diaz is also with *Universidad del Magdalena*, Colombia.

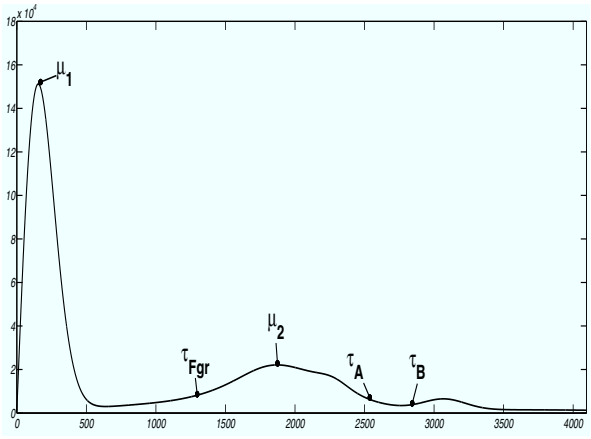

Fig. 1: Bi-modal function with modes μ_1 and μ_2 and multiple thresholds: $\tau_{\text{Fgr}}, \tau_A$ and τ_B

.

After ABTS produces these smooth histogram envelopes, it then localizes the first and second modes, μ_1 and μ_2. Typically, the edema presents high intensity signal on FLAIR and T2, and the gadolinium-enhanced lesion presents high T1C intensities. Furthermore, most tumors have low signal intensity on T1. Table I summarizes some patterns that we have observed in brain tumor MRIs. These observations lead us to threshold the images after the second mode μ_2 to separate areas of high intensities from the rest of the brain tissues.

TABLE I: Signal intensity for tumors on MRIs.

	Edema	**Gadolinium-enhanced Lesion**	**Skull**
T1	Low	Low	High
T1C	Low	High	High
T2	High	High	High
FLAIR	High	–	High

In particular, ABTS analyzes the first and second derivatives of the histogram envelopes after μ_2 and marks, as possible thresholds, the inflection points where the sign of the slope changes. For each modality $m \in \{\text{T1, T1C, T2, FLAIR}\}$, we define three main thresholds $\tau_A(m)$, $\tau_B(m)$ and $\tau_{Fgr}(m)$. Figure 1 illustrates the threshold locations. ABTS identifies τ_A as the point with the maximum slope change, after the second mode μ_2. This threshold highlights the skull's voxels on all the MRI modalities (T1, T1C, T2 and FLAIR). It also identifies the gadolinium-enhanced lesions on T1C, the edema on FLAIR, and ventricles, sulci and edema on T2, as shown in Figures 2 and 3.

The threshold $\tau_B(\text{FLAIR})$ is the first intensity value greater than $\tau_A(\text{FLAIR})$, where a slope change also occurs.

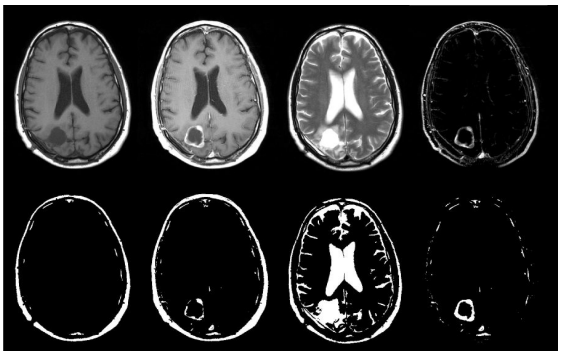

Fig. 2: Thresholding results on one slice. On the top row from left to right: T1, T1C, T2, $I_{\text{T1C-T1}}$ (as defined in Section II-D). On the bottom row from left to right, the thresholding results for $\tau_A(\text{T1}), \tau_A(\text{T1C}), \tau_A(\text{T2})$ and the enhanced lesion from $I_{\text{T1C-T1}}$.

Fig. 3: Thresholding results on one slice from FLAIR. From left to right: the slice in FLAIR, the result of thresholding with $\tau_{\text{Fgr}}(\text{FLAIR})$, the results obtained by thresholding with $\tau_A(\text{FLAIR})$ and $\tau_B(\text{FLAIR})$.

ABTS localizes this threshold in FLAIR. Figure 3 shows an example of the results obtained by thresholding FLAIR with $\tau_A(\text{FLAIR})$ and $\tau_B(\text{FLAIR})$. Both thresholds yield images containing part of the skull and edema. The image generated by $\tau_A(\text{FLAIR})$ is taken as the geodesic mask and the image generated by $\tau_B(\text{FLAIR})$ is taken as the marker set for the geodesic dilation operator [6]; see Section II-C.

The threshold τ_{Fgr} is localized in FLAIR histogram, which corresponds to the first slope change found when descending the curve from μ_2 on the left side. This threshold selects voxels corresponding to brain tissues and skull, excluding ventricles, sinuses, and sulci. Figure 3 shows an image thresholded with τ_{Fgr}.

We represent the 3D image associated with a MRI modality m, $I(m) : \Re^3 \mapsto \Re$ which gives an intensity value for each (x, y, z) point. We can use this and a threshold $\tau \in \Re$ to define a 3D mask

$$M(m, \tau)[\boldsymbol{x}] = \begin{cases} 1 & \text{if} \quad I(m)[\boldsymbol{x}] > \tau, \\ 0 & \text{otherwise.} \end{cases} \tag{1}$$

We will write $M(m, \tau_A(m))$ as just $M(m, \tau_A)$. For example $M(\text{T1}, \tau_A)$ contains all the voxels whose T1 intensities are greater than $\tau_A(\text{T1})$.

Fig. 4: Edema segmentation on one slice. From left to right, the skull mask used to strip off the skull; $M(\text{FLAIR}, \tau_B)$ and $M(\text{FLAIR}, \tau_A)$ after removing the skull; $M(\text{T2}, \tau_A)$ after removing the skull, ventricles and sulci; and the edema segmentation result.

Fig. 5: GTV segmentation on one slice. From left to right: $M(\text{T1C}, \tau_A)$ and $I_{\text{T1C}-\text{T1}}$ skull stripped; the GTV segmentation result; and the edema (cyan) and GTV (red) segmentations integrated.

B. Skull Segmentation

ABTS extracts a first approximation of the skull location by selecting the biggest 3D-connected component from $M(\text{T1}, \tau_A)$, then complementing it with $M(\text{T1C}, \tau_A)$ to produce a mask M_{skull} containing only the skull. This mask is removed from all the images *i.e.*, all of the subsequent masks consider just the volume within the skull. Figure 4 illustrates the skull mask obtained for one slice.

C. Edema Segmentation

The two masks $M(\text{FLAIR}, \tau_A)$ and $M(\text{FLAIR}, \tau_B)$ contain voxels corresponding to the tumor edema. ABTS applies a geodesic dilation operator where $M(\text{FLAIR}, \tau_B)$ is the marker and $M(\text{FLAIR}, \tau_B)$ is the geodesic mask [6]. As illustrated in Figures 3 and 4, in $M(\text{FLAIR}, \tau_B)$ the edema is less defined in comparison to $M(\text{FLAIR}, \tau_A)$. However, $M(\text{FLAIR}, \tau_A)$ often contains small regions that do not belong to the tumor but are still often 3D-connected, while $M(\text{FLAIR}, \tau_B)$ provides less information but has fewer of these small regions. For this reason, ABTS takes the edema from $M(\text{FLAIR}, \tau_B)$ as a seed in the geodesic dilation process, until reaching the edema area in $M(\text{FLAIR}, \tau_A)$.

Sometimes $M(\text{FLAIR}, \tau_A)$ does not identify the edema completely because the presence of cyst and necrosis perturb the signal intensity in the FLAIR image. To overcome this challenge, ABTS also extends the seeds by geodesic dilation over $M(\text{T2}, \tau_A)$. The geodesic dilation is performed after eliminating ventricles and sulci using $M(\text{T2}, \tau_A) \cap M(\text{FLAIR}, \tau_{\text{Fgr}})$. As the τ_{Fgr} threshold separates regions with low intensities (such as ventricles, sulci, sinuses, etc.) from tissues and skull, the image resulting from the intersection contains only voxels that correspond to the edema and some other isolated small areas with high intensity values in T2. Thus, the geodesic dilation operator is able to complement the initial edema from FLAIR with information provided by T2 as shown in Figure 4.

D. GTV Segmentation

Although τ_A(T1C) helps to identify the GTV, we complement this initial segmentation with information extracted from $I_{\text{T1C-T1}} = \text{T1C} - \text{T1}$, which is the image formed by a voxel-wise subtraction of the intensities of T1 from T1C; see Figure 2 and Figure 5. At this stage, ABTS does the following:

1) Standardize the intensity values of T1 and T1C to a common intensity scale by using the method proposed in Nyúl and Udupa [10].
2) Select from $I_{\text{T1C}-\text{T1}}$ the voxels with high intensities that are 3D-connected with the GTV from $M(\text{T1C}, \tau_A)$ and the edema mask obtained in the previous stage. Figure 5 illustrates the result of this step.

ABTS standardizes the intensity values to cancel areas that correspond to the healthy tissue and to enhance voxels corresponding to the enhanced contrast.

III. SEGMENTATION RESULTS

A. Materials

In this work, we used a MRI dataset from patients with glioblastoma, at different stages, treated at the Cross Cancer Institute (CCI) in Alberta, Canada. We developed ABTS using sixty patient cases, each containing only axial slices, in each of the four sequences T1, T1C, T2 and FLAIR, that were acquired with a 1.5T MR Philips Intera Achieva scanner using a resolution of 512×512 voxels with 21 to 25 slices (varying for different patients), and with a spatial resolution of $1 \times 1 \times 5$ mm. For each patient, the four sequences were acquired at the same imaging session without moving the patient. All MRI data were previously stripped of all patient personal information. The use of this MRI data set for this work is approved by a research ethic board at the University of Alberta.

We implemented ABTS using MATLAB and Ubuntu Mint on a Laptop with 1.73 GHz quad core $Intel^{®}$ processor and 6GB RAM.

B. Evaluation

A team of radiation oncologists from CCI hand-segmented edema and the GTV for sixteen random cases, which were different from the sixty used during the development stage. For each image, we then estimated the similarity between the mask M segmented by our method and the corresponded image E segmented by the experts, using the Dice coefficient:

$$D(M, E) = (2 \times \text{TP})/((2 \times \text{TP}) + \text{FP} + \text{FN}) \qquad (2)$$

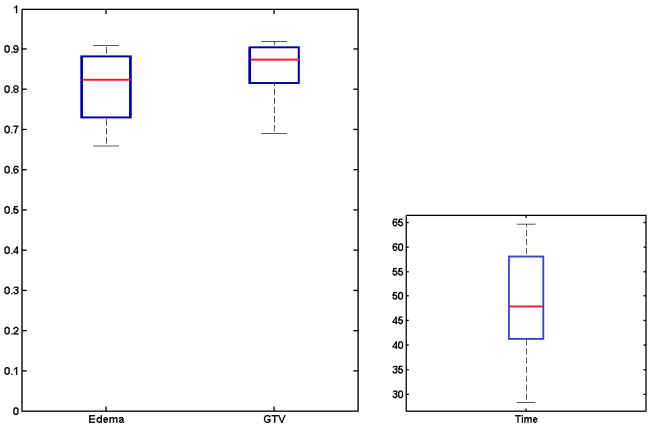

(a) Dice coefficients boxplot (b) Time boxplot

Fig. 6: (a) ABTS performance: Dice coefficient boxplots for edema and GTV; (b) segmentation times for the data set.

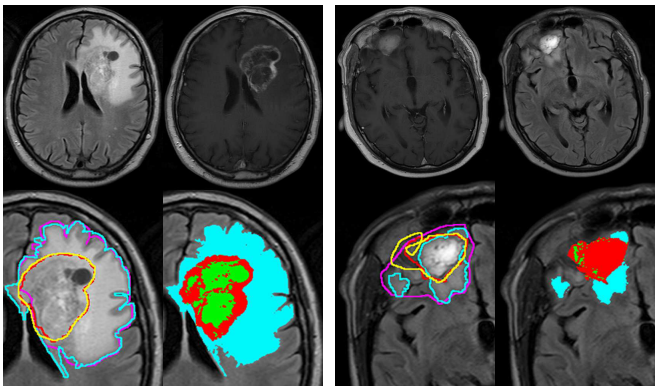

(a) An slice form the best segmentation (b) An slicec from the worst segmentation

Fig. 7: The top images in (a) and (b) are the original slices in FLAIR and T1C. On the bottom left, edema: manual in magenta and automatic in cyan lines; GTV: manual in yellow and automatic in red lines.The bottom right images are only the edema and GTV automatic segmentations.

where TP, FP and FN are respectively the number of voxels that are true positive, false positive and false negative.

Figure 6a shows a box plot of the Dice coefficients obtained for the sixteen evaluation cases, for both the edema and GTV segmentations. The average Dice coefficients for Edema and GTV are 81% and 85% respectively. Figure 7 shows slice examples of the segmentations obtained for the best and the worst evaluated cases.

We see that ABTS did extremely well, on essentially every volume. The few exceptions happened when the images from different modalities did not satisfy the rules given in Table I. The worst case, Figure 7b is caused by the presence of high intensity levels covering the tumor area in some slices in the T1 sequence; this can be fixed by a better tuning of the MRI machine.

The average segmentation time is 49.18 seconds over the 60 cases of the dataset, see Figure 6b.

IV. CONCLUSION

Although the image set selected to evaluate ABTS includes some challenging cases, the average Dice coefficients of 81% and 85% show extremely high overlap between the manual and automatic segmentations for edema and GTV; these accuracies are comparable to the average dispersion between two trained radiation oncologists [11]. ABTS is also very fast, with an average time of 49.18 seconds for segmentation.

ABTS segments the four image sequences separately and connects components intersected in 3D, therefore it is able to deal with cases with slight rotation. As the four sequences (T1, T1C, T2 and Flair) for each patient were acquired at the same session without moving the patient, we did not need to deal with registration issues related to translation and scaling.

This paper presents a fast, automatic and accurate method for segmenting brain tumors. As it automatically identifies thresholds based on the histograms of intensities present in the images, the ABTS method is easily able to effectively segment images produced from different protocols and scanners.

REFERENCES

[1] G. Mazzara, R. Velthuizen, J. Pearlman, H. Greenberg, and H. Wagner, "Brain tumor target volume determination for radiation treatment planning through automated MRI segmentation," *Int. J. Radiat. Oncol.*, vol. 59, 2004.

[2] D. Pham, C. Xu, and J. Prince, "Current methods in medical image segmentation," *Annu. Rev. Biomed. Eng.*, vol. 2, 2000.

[3] P. Cattin, M. Harders, J. Hug, R. Sierra, and G. Szekely, "Computer-supported segmentation of radiological data," in *Biomedical Image Analysis - Segmentation Models*, 2005.

[4] I. Bankman, *Handbook of Medical Image: Processing and Analysis*, 2008.

[5] J. Bushberg, A. Seibert, E. Leidholdt, and J. Boone, *The Essential Physics of Medical Imaging*, 2nd ed., Dec. 2001.

[6] P. Soille, *Morphological Image Analysis: Principles and Applications*. Springer, 2010.

[7] M. Brummer, R. Merserau, R. Eisner, and R. Lewine, "Automatic detection of brain contours in MRI data sets," vol. 12, June 1993.

[8] A. Savitzky and M. Golay, "Smoothing and Differentiation of Data by Simplified Least Squares Procedures," *Anal. Chem.*, vol. 36, 1964.

[9] P. Persson and G. Strang, "Smoothing by Savitzky-Golay and Legrend Filters," in *Mathematical Systems Theory in Biology, Communications, Computation and Finance*, 2003.

[10] L. Nyúl and J. Udupag, "On standardizing the MR image intensity scale," *Magn. Reson. Med.*, vol. 42, 1999.

[11] M. Schmidt, "Automatic brain tumor segmentation," Master's thesis, University of Alberta, 2005.